

## EFFECT OF ENVIRONMENT ON GALAXIES MASS-SIZE DISTRIBUTION: UNVEILING THE TRANSITION FROM OUTSIDE-IN TO INSIDE-OUT EVOLUTION

MICHELE CAPPELLARI

Sub-department of Astrophysics, Department of Physics, University of Oxford, Denys Wilkinson Building, Keble Road, Oxford,  
OX1 3RH, UK

*The Astrophysical Journal Letters. Received 2013 September 4; accepted 2013 September 27*

### ABSTRACT

The distribution of galaxies on the mass-size plane as a function of redshift or environment is a powerful test for galaxy formation models. Here we use integral-field stellar kinematics to interpret the variation of the mass-size distribution in two galaxy samples spanning extreme environmental densities. The samples are both identically and nearly mass-selected (stellar mass  $M_* \gtrsim 6 \times 10^9 M_\odot$ ) and volume-limited. The first consists of nearby field galaxies from the ATLAS<sup>3D</sup> parent sample. The second consists of galaxies in the Coma Cluster (Abell 1656), one of densest environments for which good resolved spectroscopy can be obtained. The mass-size distribution in the dense environment differs from the field one in two ways: (i) spiral galaxies are replaced by bulge-dominated disk-like fast-rotator early-type galaxies (ETGs), which follow the *same* mass-size relation and have the *same* mass distribution as in the field sample; (ii) the slow rotator ETGs are segregated in mass from the fast rotators, with their size increasing proportionally to their mass. A transition between the two processes appears around the stellar mass  $M_{\text{crit}} \approx 2 \times 10^{11} M_\odot$ . We interpret this as evidence for bulge growth (outside-in evolution) and bulge-related environmental quenching dominating at low masses, with little influence from merging, while significant dry mergers (inside-out evolution) and halo-related quenching driving the mass and size growth at the high-mass end. The existence of these two processes naturally explains the diverse size evolution of galaxies of different masses and the separability of mass and environmental quenching.

*Keywords:* galaxies: clusters: individual (Abell 1656) — galaxies: evolution — galaxies: formation — galaxies: structure

### 1. INTRODUCTION

Galaxy stellar masses and sizes are powerful observables to study galaxy evolution. They vary with time or environment, during the hierarchical galaxy growth. But growth rates depend on the assembly process (e.g. Khochfar & Silk 2006; Naab et al. 2009; Hopkins et al. 2010). A theme emerging from both theory and observations is a dichotomy between the redshift and environmental evolution of galaxy sizes as a function of stellar mass.

On one hand the passive early-type galaxies (ETGs) with stellar masses  $M_* \gtrsim 10^{11} M_\odot$  are found to be, on *average*, smaller and denser at redshift  $z \sim 2$ . This results comes from both photometry (e.g. Daddi et al. 2005; Trujillo et al. 2006; van Dokkum et al. 2008) and stellar velocity dispersion (e.g. Cappellari et al. 2009; Cenarro & Trujillo 2009; van de Sande et al. 2013). On the other hand lower-mass disks, show no significant size evolution out to  $z \sim 1$  (e.g. Barden et al. 2005; Sargent et al. 2007) and little evolution out to  $z \sim 3$  (Nagy et al. 2011).

A dichotomy is also seen in the evolution of galaxy profiles. Massive passive galaxies (present day  $M_* \approx 3 \times 10^{11} M_\odot$ ) build their mass mostly inside-out, by gradually assembling a stellar halo around a compact spheroid (van Dokkum et al. 2010). In contrast, lower mass star forming systems (present day  $M_* \approx 5 \times 10^{10} M_\odot$ ) indicate and early bulge growth followed by a modest but uniform growth in size at all radii (van Dokkum et al. 2013).

An increase in the galaxies number density has a similar effect on galaxy properties as time evolution. This is

likely because at high redshift the abundance of massive halos declines and fewer galaxies are in clusters than locally. Overdensities transform spirals into passive ETGs (Dressler 1980) and increase mean galaxy masses (Kauffmann et al. 2004). In apparent contrast to redshift evolution however, both spirals and ETGs follow nearly the same mass-size relations in different environments (e.g. Maltby et al. 2010; Huertas-Company et al. 2013; Poggianti et al. 2013). Although some size differences were reported at  $z \sim 1$ , they are either small (25% in Cooper et al. 2012), or only affect massive galaxies ( $M_* \gtrsim 2 \times 10^{11} M_\odot$  in Lani et al. 2013).

Here we want to understand the origin of the observed trends, using the exquisite detail on the fossil record of galaxy formation one can obtain only for nearby galaxies. We combine available integral-field stellar kinematics and Hubble Space Telescope (HST) photometry of the inner surface brightness profiles to robustly recognize the merger history the galaxies have experienced. We study two extreme environments which differ by almost three orders of magnitude in galaxy number density. We show that a simple picture can reconcile the trends of galaxy sizes with the detailed fossil record of galaxy formation.

### 2. SAMPLE AND DATA

#### 2.1. Selection

The galaxies in both our low-density and high-density samples are identically selected from the 2MASS (Skrutskie et al. 2006) Extended Source Catalog (XSC) for having total absolute magnitude (from XSC keyword `k_m_ext`)  $M_{K_s} < -21.5$  mag ( $M_* \gtrsim 6 \times 10^9 M_\odot$ ).

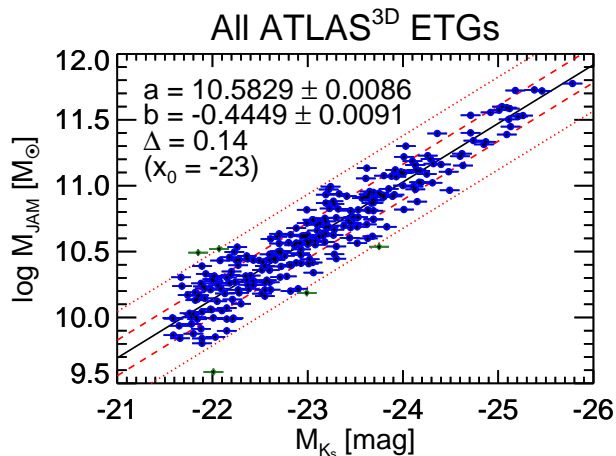


**Figure 1.** From  $K_s$  luminosity to stellar mass. The dynamical mass  $M_{\text{JAM}} \approx M_*$  is plotted against the total luminosity  $M_{K_s}$ . The best fitting relation (solid line) and the  $1\sigma$  and  $2.6\sigma$  bands are also shown with the dashed and dotted lines respectively. The green filled diamonds were automatically excluded from the fit. The best-fitting linear parameter and errors are printed, together with the observed scatter  $\Delta$  and pivot magnitude  $x_0$ .

Our low-density (field) sample consists of all 743 galaxies in the ATLAS<sup>3D</sup> *parent* sample (Cappellari et al. 2011a) not belonging to the Virgo cluster according to that paper. This provides a clean group/field environment as shown in Cappellari et al. (2011b). The sample is volume-limited within a distance of 42 Mpc and 98% complete (sec. 2.1 of Cappellari et al. 2013b). The median number density of this sample is  $\log \Sigma_3 = -0.5$  ( $\text{Mpc}^{-2}$ ) using the 3rd nearest neighbor estimator determinations from Cappellari et al. (2011b).

Our high-density (cluster) sample consists of all 160 cluster-member galaxies within a circle of area  $1 \text{ deg}^2$  centered on the core of the Coma cluster (Abell 1656). The center was assumed as the midpoint between the two central galaxies NGC 4874 and NGC 4884 which nearly coincides with the peak of the X-ray emission (White et al. 1993). We adopted a Coma cluster distance of 100 Mpc (see Carter et al. 2008). At our luminosity the XSC is essentially complete but, after visual inspection of SDSS images of the cluster, we manually added the five galaxies NGC 4871, NGC 4872, NGC 4882 (=NGC 4886), PGC 044644 and PGC 044651, which were likely missed for lying within the stellar halo of the central galaxies.

All the 2MASS selected galaxies in Coma have a redshift in either SDSS or the NASA Extragalactic Database. We removed the only 12 galaxies with recession velocity  $V_{\text{hel}} > 11000 \text{ km s}^{-1}$ , providing a complete sample of cluster-member galaxies within the given cylinder. The selection radius of 1.0 Mpc is about 1/3 of the dark halo virial radius (Lokas & Mamon 2003). The Coma sample has a median density  $\log \Sigma_3 = 2.0$  ( $\text{Mpc}^{-2}$ ), when computed in identical manner as for ATLAS<sup>3D</sup>.

## 2.2. Galaxy sizes and masses

All galaxy sizes are homogeneously taken from the XSC. Effective radii  $R_e^{\text{maj}}$  are defined as the major axis of the isophote enclosing half of the *total* galaxy light in  $J$ -band (XSC keyword `j_r_eff`) which has better  $S/N$ . The use of  $R_e^{\text{maj}}$  is needed to remove the strong inclina-

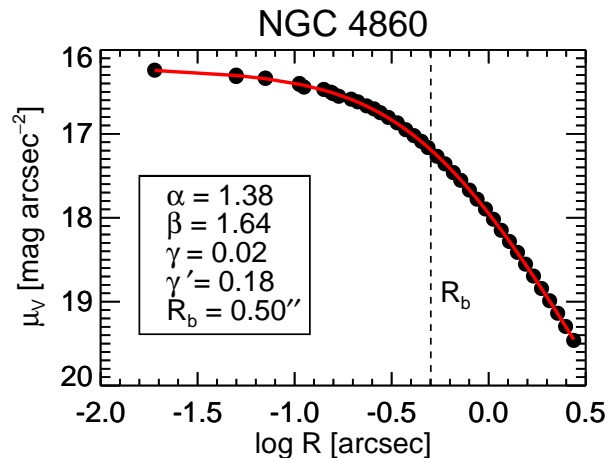


**Figure 2.** Nuker-law fit to the surface brightness profile of the Coma slow rotator NGC 4860. The surface brightness profile of the galaxy (filled circles) is plotted against the radius. The best fitting relation is overlaid with the red solid line and the corresponding parameters are written in the caption. The logarithmic slope  $\gamma' = 0.18 < 0.3$  at  $R = 0''.1$  identifies NGC 4860 as a core galaxy.

tion dependence of the circularized  $R_e$ , for disk galaxies (Cappellari et al. 2013a). The XSC effective radii are among the most reproducible relative size measures (Cappellari et al. 2013a). However the absolute normalization of  $R_e^{\text{maj}}$  depends on the quality of the data. We define  $R_e^{\text{maj}} = 1.61 \times j\_r\_eff$  to match the  $R_e^{\text{maj}}$  of Cappellari et al. (2013a) for the galaxies in common, making our results directly comparable.

Sizes measured via growth curves saturate near the FWHM of the 2MASS PSF, which is  $\sim 1.5 \text{ kpc}$  at Coma. We corrected `j_r_eff` using the following formula which we found via simulations is 5% accurate for an  $R^{1/4}$  profile, a Gaussian PSF, and  $R_e^{\text{true}} > \sigma_{\text{PSF}}/2$ , with weak dependence on the Sersic index and flattening

$$(R_e^{\text{true}})^2 = (R_e^{\text{obs}})^2 - (1.45 \times \sigma_{\text{PSF}})^2. \quad (1)$$

This is approximate but is not critical for our conclusions as it only affects the few smallest Coma galaxies.

Galaxy masses derived from stellar population necessarily ignores systematic variations of about a factor of two in the stellar Initial Mass Function (e.g. Cappellari et al. 2012; Conroy & van Dokkum 2012). For this reason our masses are based on  $K_s$ -band luminosities:

$$\log_{10} M_* \approx 10.58 - 0.44 \times (M_{K_s} + 23). \quad (2)$$

This was fitted (Fig. 1) using the LTS\_LINEFIT routine of Cappellari et al. (2013a) to the ATLAS<sup>3D</sup> dynamical masses  $M_{\text{JAM}}$  from Cappellari et al. (2013a). We then assumed  $M_* = M_{\text{JAM}}$  as discussed in sec. 4.3 of Cappellari et al. (2013a). Our relation is fitted to ETGs and may become inaccurate for spirals. However Williams et al. (2009) find the  $(M/L)_{K_s}$  of spirals and ETGs does not differ by more than  $\sim 50\%$ . None of our conclusions depend on this approximation.

## 3. RECOGNIZING MERGING HISTORY

We want to robustly recognize genuine spheroidal-like early-type galaxies that are the likely result of dry mergers from inclined disk-like systems. Integral-field stellar kinematics was shown to provide an excellent discrimination of these two classes of galaxies, nearly independently

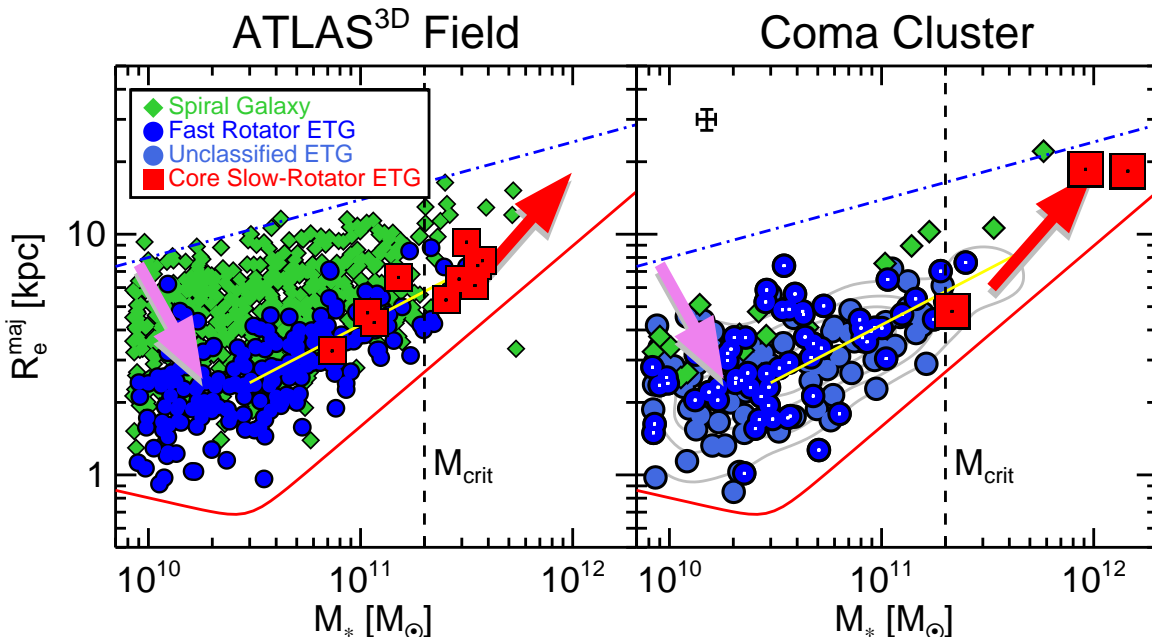


**Figure 3.** Mass-size distributions in extreme environments. The left panel shows the field subsample of the ATLAS<sup>3D</sup> sample of nearby galaxies. The right panel shows an identically-selected sample of Coma cluster members. A representative error bar is indicated. The gray contours in the right panel show for reference the kernel density estimate for the ETGs distribution in the left panel, while the yellow line is the corresponding mean relation (from fig. 2 of Cappellari et al. 2013b). For references the blue dash-dotted line and the thick red line indicate the upper limit of the spiral galaxies and the lower limit for ETGs from Cappellari et al. (2013b). The critical mass  $M_{\text{crit}}$  is marked by the black dashed line. The magenta arrow qualitatively indicates the evolutionary track due to bulge growth and quenching, with little mass increase. The red arrow shows the models prediction track for major dry merging with a factor 3 mass increase.

of inclination. The two classes were called slow and fast-rotator ETGs respectively (Emsellem et al. 2007; Cappellari et al. 2007).

Another signature which was shown to indicate dry merger remnants is the presence of a core or light deficit in the inner surface-brightness profile (e.g. Kormendy et al. 2009). Although the kinematic approach is more robust, in many cases the core and slow-rotator classifications agree as expected (Lauer 2012). However there are important cases where either core galaxies or slow-rotator ETGs appear clearly disk-like and inconsistent with being dry-merger remnants (Krajinović et al. 2013). We found that selecting only slow rotators *with core* eliminates from the class the ‘misclassified’ flat counter-rotating disks or unsettled mergers (Krajinović et al. 2011; Emsellem et al. 2011) and appears to unambiguously indicate dry-merger remnants only. For this reason here we use core slow-rotator galaxies to define dry mergers remnants.

For the ATLAS<sup>3D</sup> sample we take the fast/slow rotator separation from Emsellem et al. (2011) and the cusp/core one from Krajinović et al. (2013). For the Coma sample we used the fast/slow rotator classes recently derived from integral-field spectroscopy (IFS) by Houghton et al. (2013). The three slow rotators ( $C = 3$  in their table 1), NGC 4874, NGC 4884 (=NGC 4889) and NGC 4860, all have a core. For the first two objects the core classification is given in Lauer et al. (2007), and we classified the third one from HST photometry (Fig. 2). Unlike for the ATLAS<sup>3D</sup> sample, the Coma IFS observations are not complete but cover 27 ETGs representative of the population within the innermost 15 arcmin from the cluster center. We classified 39 additional objects as fast rotator from their apparent flattening: all galaxies flatter than

$\varepsilon > 0.4$  (from XSC keyword `sup_ba`) must be fast rotators as shown by Emsellem et al. (2011). In the next section we discuss why this subsample allows us to reach general conclusions for the entire cluster.

#### 4. MASS-SIZE RELATION IN EXTREME ENVIRONMENTS

The mass-size distribution for the field subset of the ATLAS<sup>3D</sup> parent sample is presented in the left panel of Fig. 3 (for the entire sample see fig. 9 of Cappellari et al. 2013b). It shows two nearly parallel sequences of spiral galaxies and fast-rotator ETGs, with the latter having smaller size at given mass. Core slow-rotators do not follow the trends of spirals and fast rotator ETGs. They lie along the mass-size relation defined by fast rotators but are only present above  $M_* \gtrsim 10^{11} M_{\odot}$  (Krajinović et al. 2013) and start dominating the ETGs population above  $M_{\text{crit}} \approx 2 \times 10^{11} M_{\odot}$ , where a number of galaxy properties abruptly change (Cappellari et al. 2013b).

The mass-size relation for the galaxies in the Coma cluster is shown in the right panel of Fig. 3. We also quantify the cluster/field mass and size distributions in Fig. 4. The following results are obvious: (i) spiral galaxies in Coma are replaced by fast rotator ETGs which follow the *same* mass-size relation and have the *same* mass distribution as the field sample; (ii) slow rotator ETGs in Coma lie above  $M_{\text{crit}}$  and the two largest galaxies appear segregated in mass from the fast rotators, with their size increasing proportionally to their mass. The two massive slow rotators stand out for sitting near the center of the cluster, while the third one lies along a slight overdensity (Fig. 5 right).

Although the Coma IFS observations do not sample the entire cluster, they do sample most of its densest part (Fig. 5 right). The fact that no core slow rotator was found below  $M_{\text{crit}}$  in the densest parts, makes it unlikely

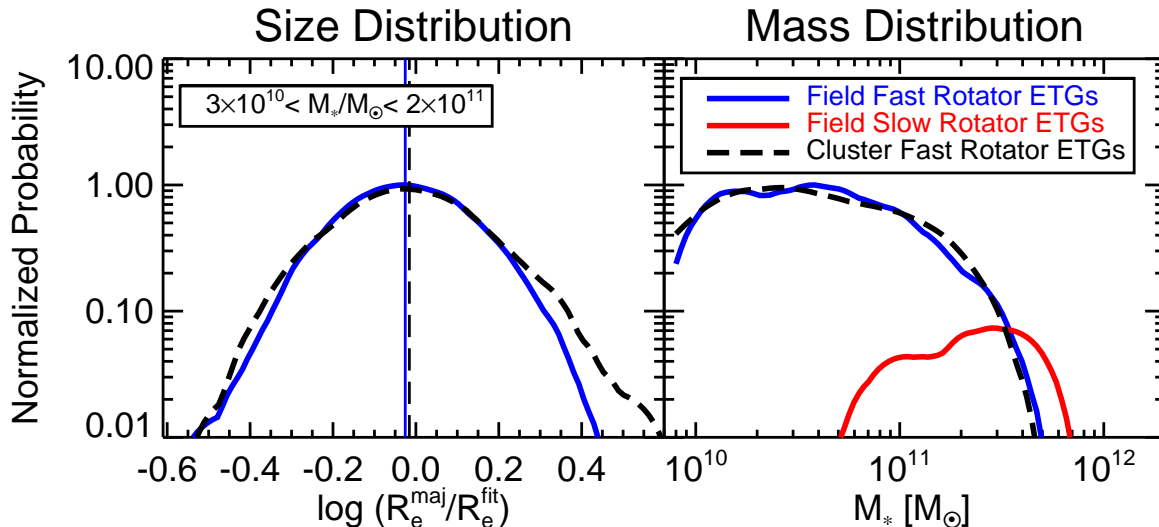


**Figure 4.** Size and mass distributions of fast rotator ETGs in the field and cluster samples. In the left panel a normalized kernel density estimate of the probability distribution, is plotted as a function of the logarithm of the ratio between the observed  $R_e^{\text{maj}}$  and the value predicted by the best-fitting relation  $(R_e^{\text{fit}}/\text{kpc}) = 4.2 \times [M_*/(10^{11} M_\odot)]^{0.46}$  (yellow line in Fig. 3). This is done to remove the significant size variation within the selected mass interval  $3 \times 10^{10} < M_*/M_\odot < 2 \times 10^{11}$ . The vertical lines indicate the biweight mean of the distributions which differ by just 4%. The tail at larger sizes in the cluster sample is likely due to red spirals, which are more common in clusters and are easily confused with ETGs. This asymmetry may explain some of the reported size increase of passive galaxies in denser environments. The right panel shows the very similar distributions of galaxy masses. The core slow-rotators in the field are shown in red.

that others may be found in the rest of the cluster. This is because previous IFS studies in the Virgo (Fig. 5 left; Cappellari et al. 2011b), Abell 1689 (D’Eugenio et al. 2013) and Coma cluster (Houghton et al. 2013) have shown core slow rotators to be strongly concentrated towards the densest part of the clusters. Even making the incorrect and extreme assumption that the distribution of slow rotators is independent of environment, using the hypergeometric distribution we can say that if there were more than just three slow rotators among the ETGs without IFS, we would have a  $> 50\%$  chance of observing at least one. We find no slow rotator below  $M_{\text{crit}}$ .

## 5. DISCUSSION

### 5.1. Two formation processes

Our work relies on our ability to distinguish, within the ETGs class, the relics of dry mergers, the core slow rotators, from inclined passive disks with a range of bulge fractions, the fast rotators. The comparison between the mass-size relation we observe in the field and in the core of the dense Coma cluster, reveals two distinct processes transforming galaxies in clusters: (i) Spirals transform into fast rotator ETGs while decreasing in  $R_e^{\text{maj}}$  with little mass variation, while (ii) slow rotators increase in  $R_e^{\text{maj}}$  roughly proportionally to their  $M_*$ , segregating in mass from the fast rotators.

As discussed in Cappellari et al. (2013b), the decrease of  $R_e^{\text{maj}}$  from the spirals to the fast rotator ETGs traces the bulge growth, concentrating mass at smaller radii. The fact that fast rotator ETGs have smaller  $R_e^{\text{maj}}$  than spirals shows that the environmental quenching of star formation is associated to the bulge growth (and likely some disk fading). The fact that the mass distribution of fast rotators is the same in both the field and in Coma shows that mass increased insignificantly during the environmental transformation (see also Carollo et al. 2013).

Various processes can transform spirals into passive ETGs (see Boselli & Gavazzi 2006, for a review). Both

high-speed encounters within the cluster or secular evolution can drive gas towards the center, growing a bulge and producing a starburst which is subsequently quenched by some feedback (e.g. AGN or supernovae). These will combine with ram-pressure stripping of the cold gas or other forms of more gradual gas starvation.

An opposite alternative to explain the differences in the field and cluster mass-size relations would be the lack of disk growth around pre-existing spheroids in the cluster environment. The homogeneity in the dynamical structure of bulges and disks of fast rotators (Cappellari et al. 2013a), the similarity in the maximum mass of fast-rotator ETGs and spirals, and the evolution of the surface brightness profiles as a function of redshift (van Dokkum et al. 2013) seem to rule out this scenario.

The situation is completely different for the slow-rotator ETGs. Compared to the field sample, the high-density environment appears to evolve these objects along lines of  $R_e^{\text{maj}} \propto M_*$  in the mass-size plane. The two most massive slow rotators in Coma appear segregated in mass from the fast rotator population, with a  $\sim 5\times$  gap in  $M_*$ , which is not present in the field sample. The median mass increase for the slow rotators in Coma with respect to our field sample is about a factor three.

The size increase in approximate proportion to the mass, combined with the mass segregation of slow rotators from fast rotators in Coma, is direct evidence for major growth of slow rotators by dry mergers in the cluster environment. The observed size increase with mass is the one predicted for major (not minor) dry mergers. This is consistent with the mass versus velocity dispersion relation of nearby ETGs (Cappellari et al. 2013b; Kormendy & Bender 2013). However very massive galaxies generally have extended stellar halos which may be missed by 2MASS. Deeper observations would likely indicate larger  $R_e$  (e.g. Kormendy et al. 2009), making the size increase more consistent with the minor merging formation hypothesis (e.g. Naab et al. 2009).

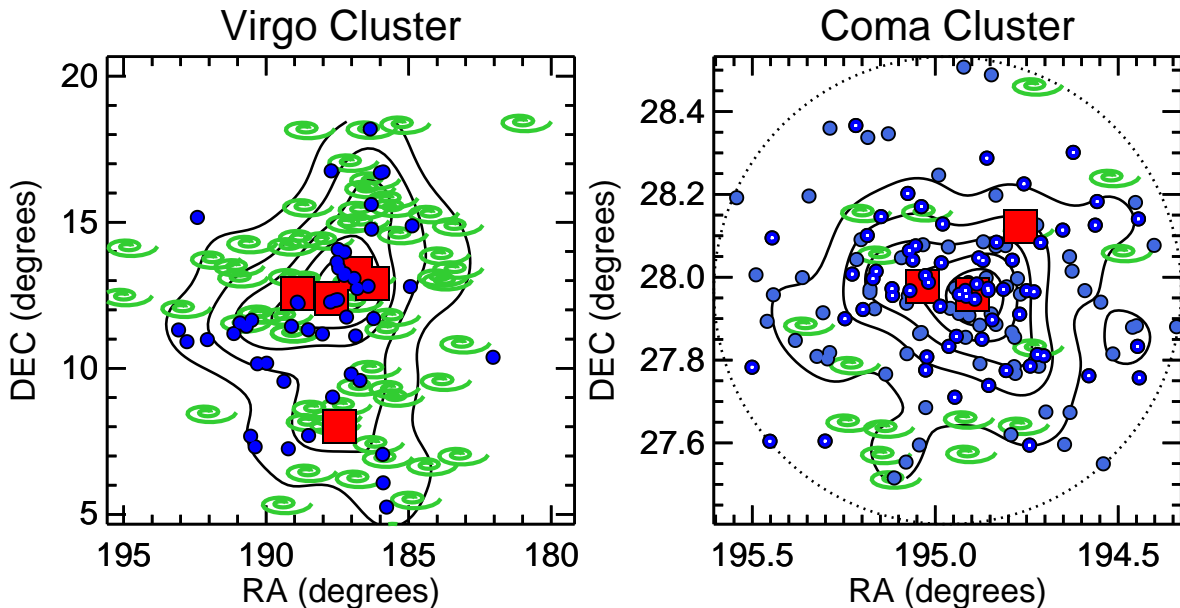


**Figure 5.** Distribution of galaxies in the Virgo and Coma clusters. Symbols are the same as in Fig. 3, except that here the spirals are shown as green spirals. The large dotted circle in the right panel is our selection limit. A kernel density estimate for the galaxy distribution is overlaid with linearly spaced contours. The spirals and fast-rotator ETGs distribution is quite different in the two panels, but in both cases the few core slow-rotators are concentrated near the density peaks.

The hierarchical paradigm for galaxy formation implies that galaxies experience a variety of environments during their evolution. Core slow-rotators do not need to form in clusters, as illustrated by our field sample. They likely form in efficient starburst in the high-redshift Universe and, due to their large masses, they sink to the center of groups via dynamical friction. When groups merge to form massive clusters, slow rotators again sink towards the center where they merge to form more massive slow rotators. The same cannot happen to fast rotators, which have too small masses to efficiently sink to the center and too fast velocities to merge. They are quenched by the cluster but essentially don’t change their mass. This picture is broadly consistent with theoretical studies (e.g. De Lucia et al. 2012).

A progenitor of the Coma cluster may have looked like the less massive Virgo cluster which contains four core slow-rotators closely packed within its central core (sub-cluster A), surrounded by a swarm of fast rotators and a much larger fraction of spirals than in Coma (Fig. 5). Another core slow rotator lies at the center of Virgo sub-cluster B (see Cappellari et al. 2011b). Consistently with this scenario is the fact that the Virgo core slow-rotators are more numerous than in Coma and not yet segregated in mass from the fast rotators.

### 5.2. Explaining mass, environment and redshift trends

The existence of two distinct evolutionary paths for fast and slow rotator ETGs naturally explains a number of previously reported empirical trends, which seems different manifestations of this phenomenon.

Our result explains why galaxy quenching appears to depend in a separable way on mass and environment (Peng et al. 2010; Smith et al. 2012). Fig. 3 shows that the “environment quenching” consist of the transformation of spirals into fast rotator ETGs with similar masses, while “mass quenching” is a combination of the two facts that: (i) when spirals transform into fast ro-

tators, quenching is driven by bulge mass fraction, irrespective of environment (Cappellari et al. 2013b), and (ii) when slow rotator ETGs grow in mass they quench above  $M_{\text{crit}} \approx 2 \times 10^{11} M_{\odot}$ , irrespective of environment.

Two distinct processes, “bulge-driven” and a “halo-driven” quenching, were recently proposed to explain the distribution of galaxy properties, stellar population and gas content on the mass-size relation of the ATLAS<sup>3D</sup> sample (Cappellari et al. 2013b) and the link between star formation and central density in galaxies (Cheung et al. 2012). Our study confirms and clarify the nature of the two processes involved.

The different formation paths of fast and slow rotator ETGs described previously, appears related with the different “outside-in” versus “inside-out” redshift evolution of sizes and profiles of galaxies with masses below/above  $M_{\text{crit}}$  (e.g. van Dokkum et al. 2010, 2013). Our results suggests one should identify the first class with the progenitors of fast rotators and the second one with the progenitors of the slow rotator ETGs.

The lack of environmental size variation we observe for fast rotators and the strong size increase of slow rotators explains some contrasting results on the environmental size dependence, as this depends on the fraction of fast and slow rotators in the samples.

The bulge growth versus dry merging distinction also explains the fact that, while the ratio of fast rotators to spirals increases strongly with number density, there is no clear trend in the ratio of slow rotators to fast rotators, except in the center of clusters (Cappellari et al. 2011b). This result was shown to hold up to the densest environments (Scott et al. 2012; D’Eugenio et al. 2013; Houghton et al. 2013).

I thank the referee for a very useful report. I acknowledge support from a Royal Society University Research Fellowship.

## REFERENCES

- Barden, M., Rix, H.-W., Somerville, R. S., et al. 2005, *ApJ*, 635, 959
- Boselli, A., & Gavazzi, G. 2006, *PASP*, 118, 517
- Cappellari, M., Emsellem, E., Bacon, R., et al. 2007, *MNRAS*, 379, 418
- Cappellari, M., di Serego Alighieri, S., Cimatti, A., et al. 2009, *ApJ*, 704, L34
- Cappellari, M., Emsellem, E., Krajnović, D., et al. 2011a, *MNRAS*, 413, 813
- . 2011b, *MNRAS*, 416, 1680
- Cappellari, M., McDermid, R. M., Alatalo, K., et al. 2012, *Nature*, 484, 485
- Cappellari, M., Scott, N., Alatalo, K., et al. 2013a, *MNRAS*, 432, 1709
- Cappellari, M., McDermid, R. M., Alatalo, K., et al. 2013b, *MNRAS*, 432, 1862
- Carollo, C. M., Bschorr, T. J., Renzini, A., et al. 2013, *ApJ*, 773, 112
- Carter, D., Goudfrooij, P., Mobasher, B., et al. 2008, *ApJS*, 176, 424
- Cenarro, A. J., & Trujillo, I. 2009, *ApJ*, 696, L43
- Cheung, E., Faber, S. M., Koo, D. C., et al. 2012, *ApJ*, 760, 131
- Conroy, C., & van Dokkum, P. G. 2012, *ApJ*, 760, 71
- Cooper, M. C., Griffith, R. L., Newman, J. A., et al. 2012, *MNRAS*, 419, 3018
- Daddi, E., Renzini, A., Pirzkal, N., et al. 2005, *ApJ*, 626, 680
- De Lucia, G., Weinmann, S., Poggianti, B. M., Aragón-Salamanca, A., & Zaritsky, D. 2012, *MNRAS*, 423, 1277
- D'Eugenio, F., Houghton, R. C. W., Davies, R. L., & Dalla Bontà, E. 2013, *MNRAS*, 429, 1258
- Dressler, A. 1980, *ApJ*, 236, 351
- Emsellem, E., Cappellari, M., Krajnović, D., et al. 2007, *MNRAS*, 379, 401
- . 2011, *MNRAS*, 414, 888
- Hopkins, P. F., Bundy, K., Hernquist, L., Wuyts, S., & Cox, T. J. 2010, *MNRAS*, 401, 1099
- Houghton, R. C. W., Davies, R. L., DEugenio, F., et al. 2013, *MNRAS* in press (doi:10.1093/mnras/stt1399)
- Huertas-Company, M., Mei, S., Shankar, F., et al. 2013, *MNRAS*, 428, 1715
- Kauffmann, G., White, S. D. M., Heckman, T. M., et al. 2004, *MNRAS*, 353, 713
- Khochfar, S., & Silk, J. 2006, *ApJ*, 648, L21
- Kormendy, J., & Bender, R. 2013, *ApJ*, 769, L5
- Kormendy, J., Fisher, D. B., Cornell, M. E., & Bender, R. 2009, *ApJS*, 182, 216
- Krajnović, D., Emsellem, E., Cappellari, M., et al. 2011, *MNRAS*, 414, 2923
- Krajnović, D., Karick, A. M., Davies, R. L., et al. 2013, *MNRAS*, 433, 2812
- Lani, C., Almaini, O., Hartley, W. G., et al. 2013, *MNRAS*, 435, 207
- Lauer, T. R. 2012, *ApJ*, 759, 64
- Lauer, T. R., Cappellari, M., Cappellari, M., et al. 2007, *ApJ*, 664, 226
- Lokas, E. L., & Mamon, G. A. 2003, *MNRAS*, 343, 401
- Maltby, D. T., Aragón-Salamanca, A., Gray, M. E., et al. 2010, *MNRAS*, 402, 282
- Naab, T., Johansson, P. H., & Ostriker, J. P. 2009, *ApJ*, 699, L178
- Nagy, S. R., Law, D. R., Shapley, A. E., & Steidel, C. C. 2011, *ApJ*, 735, L19
- Peng, Y.-j., Lilly, S. J., Kovač, K., et al. 2010, *ApJ*, 721, 193
- Poggianti, B. M., Calvi, R., Bindoni, D., et al. 2013, *ApJ*, 762, 77
- Sargent, M. T., Carollo, C. M., Lilly, S. J., et al. 2007, *ApJS*, 172, 434
- Scott, N., Houghton, R., Davies, R. L., et al. 2012, *MNRAS*, 425, 1521
- Skrutskie, M. F., Cutri, R. M., Stiening, R., et al. 2006, *AJ*, 131, 1163
- Smith, R. J., Lucey, J. R., Price, J., Hudson, M. J., & Phillipps, S. 2012, *MNRAS*, 419, 3167
- Trujillo, I., Förster Schreiber, N. M., Rudnick, G., et al. 2006, *ApJ*, 650, 18
- van de Sande, J., Kriek, M., Franx, M., et al. 2013, *ApJ*, 771, 85
- van Dokkum, P. G., Franx, M., Kriek, M., et al. 2008, *ApJ*, 677, L5
- van Dokkum, P. G., Whitaker, K. E., Brammer, G., et al. 2010, *ApJ*, 709, 1018
- van Dokkum, P. G., Leja, J., Nelson, E. J., et al. 2013, *ApJ*, 771, L35
- White, S. D. M., Briel, U. G., & Henry, J. P. 1993, *MNRAS*, 261, L8
- Williams, M. J., Bureau, M., & Cappellari, M. 2009, *MNRAS*, 400, 1665